


Article

# Optimization-Based Control for a Large-Scale Electrical Vertical Take-Off and Landing during an Aircraft's Vertical Take-Off and Landing Phase with Variable-Pitch Propellers

Luyuhang Duan <sup>1</sup> , Yunhan He <sup>1,\*</sup>, Li Fan <sup>1,2,\*</sup>, Wei Qiu <sup>1</sup>, Guangwei Wen <sup>2</sup> and Yun Xu <sup>1</sup>

<sup>1</sup> College of Control Science and Engineering, Zhejiang University, Hangzhou 310027, China; 12232048@zju.edu.cn (L.D.); 0622215@zju.edu.cn (W.Q.); xuyunxy@zju.edu.cn (Y.X.)

<sup>2</sup> Huzhou Institute, Zhejiang University, Huzhou 313000, China; wengw@hizju.org

\* Correspondence: heyunhan@zju.edu.cn (Y.H.); fanli77@zju.edu.cn (L.F.)

**Abstract:** The UAV industry has witnessed an unprecedented boom in recent years. Among various kinds of UAV platforms, the vertical take-off and landing (VTOL) aircraft with fixed-wing configurations has received more and more attention due to its flexibility and long-distance flying abilities. However, due to the fact that the advance ratio of regular propeller systems during the cruise phase is significantly higher than that during the VTOL phase, a variable-pitch propeller system is proposed and designed which can be applied without additional propulsion mechanisms during both flying stages. Thus, a VTOL aircraft platform is proposed based on the propulsion system constructed of variable-pitch propellers, and appropriate control manners are precisely analyzed, especially during its VTOL phase. As a basic propulsion system, a nonlinear model for variable-pitch propellers is constructed, and an optimization-based control allocation module is developed because of its multi-solution and high-order characteristics. Finally, the objective function is designed according to the stability and energy consumption requirements. Simulation experiments demonstrate that the proposed controller is able to lower energy consumption and maintain the stability of the aircraft while tracking aggressive trajectories for large-scale VTOLs with noises at the same time.

**Keywords:** VTOL; variable-pitch propellers; control allocation; energy consumption optimization; aggressive trajectory tracking



**Citation:** Duan, L.; He, Y.; Fan, L.; Qiu, W.; Wen, G.; Xu, Y.

Optimization-Based Control for a Large-Scale Electrical Vertical Take-Off and Landing during an Aircraft's Vertical Take-Off and Landing Phase with Variable-Pitch Propellers. *Drones* **2024**, *8*, 121.

<https://doi.org/10.3390/drones8040121>

Academic Editor: Shiva Raj Pokhrel

Received: 14 January 2024

Revised: 20 March 2024

Accepted: 23 March 2024

Published: 26 March 2024



**Copyright:** © 2024 by the authors. Licensee MDPI, Basel, Switzerland. This article is an open access article distributed under the terms and conditions of the Creative Commons Attribution (CC BY) license (<https://creativecommons.org/licenses/by/4.0/>).

## 1. Introduction

UAV platforms have been paid more and more attention by researchers and companies delighted with their characteristics of having a low cost, high efficiency, and minimal risk. With the intention of accomplishing long-distance flying scenarios as well as utilizing the advantage of vertically taking off and landing without an airport at the same time, the demand for UAVs with vertical take-off and landing (VTOL) capabilities has sufficiently increased. At present, VTOL UAVs have been developed in various layouts, such as a dual-system UAV [1,2], tilt-rotor UAV [3,4], tilt-wing UAV [5,6], and tail-sitter UAV [7,8], mostly using blended wings in order to adapt both the VTOL phase and the horizontally cruising phase simultaneously.

To satisfy certain needs of executing under two totally different flight modes, a number of propulsion system design schemes were proposed since normal propellers remain insufficient to provide thrust for the cruising operations of VTOLs. Some aircraft such as Pegasus PAV and VoloRegion rely on a propeller system consisting of two different sets of propellers, one set operating during a phase, which is redundant with negative effects because the aircraft only operates one flight mode at a time. Specifically, the other set of propellers usually does harm to perfect operations under the current flying phase, such as preventing the cruising flight from being faster.

In order to overcome the relatively high rotor advance ratios of normal propellers during the cruise phase, variable-pitch propellers have been designed as the propulsion system of various kinds of VTOL aircraft such as the V-22 Osprey and V-280 Valor aircraft. During the VTOL phase, the inflow angle is small, so the propellers are supposed to be equipped with small pitch angles for high-efficiency operations. Conversely, the propellers require large pitch angles to match increasingly bigger inflow angles with the aim of achieving higher efficiency during the cruise phase. Compared to regular propellers, variable-pitch propellers are helpful as they improve the efficiency of VTOL UAVs with their flexible pitch angles during both the cruise phase and VTOL phase.

Nowadays, delighted with the rapid development of electric power technology, especially the increasing power of electric motors and the growing ability of energy storage, electric VTOL (eVTOL) has become an emerging aircraft platform considering the pollution and noise produced by traditional aircraft. Different from traditional oil-driven VTOLs which rely on large fuel pipelines, 100 kg level eVTOLs succeed in making use of a distributed electric propulsion system due to the convenience and small size of electric cables. For instance, a typical eVTOL aircraft has been built by the Joby company and utilizes six electric propellers as its propulsion system. Therefore, designing and controlling distributed variable-pitch propeller systems on eVTOL aircraft are becoming meaningful and urgent research topics.

Unfortunately, current control strategies lack suitable solutions concerning satisfying flight in both phases, especially for large-scale eVTOL aircraft. Since control issues with regard to the VTOL phase of the flight envelope are mainly discussed in this paper, previous related research work considering the control of variable-pitch propellers during the VTOL phase is particularly discussed. Meanwhile, some of the scenarios where quadrotors are equipped with variable-pitch propellers are also worth focusing on as there is a lot in common between quadrotor flight and the VTOL phase flight.

Keran et al. [9] introduced methods concerning the design and analysis of passive variable-pitch propellers for VTOL UAVs. Although the passive structure decreases mechanical complexity, it sacrifices the controllability of many degrees of freedom and thus reduces the robustness and flexibility of the whole system, especially during the VTOL phase. Cutler et al. [10,11] proposed control methods based on quaternions, which offer an exquisite framework of control and trajectory generation concerning variable-pitch propellers. However, the authors concentrate on small quadrotors and their agile flights, thus maintaining four rotation speeds as high as possible in order to perform aggressive flights, leading to a waste of control resources on these four variables to a certain extent. Meanwhile, large-scale aircraft pay more attention to subjects like minimizing energy consumption and stabilizing the overall flight process, where the above control framework is not suitable to be directly applied. Xu et al. [12] introduced an aggressive trajectory tracker based on MPC and a nonlinear attitude controller for quadrotors, which is utilized on quadrotor platforms without limiting energy consumption. Unlike tiny quadrotors which are able to sacrifice some targets in order to elegantly track some aggressive trajectories, large eVTOLs should consider many more aspects of the flight, including the robustness against external disturbances and measurement noise, and energy consumption analysis. Portillo et al. [13] discussed a method to eliminate unmodeled dynamics or external disturbances at the control level, which provides a feasible solution to overcome these problems. Meanwhile, Bianchi et al. [14] addressed the energy consumption of quadrotors when tracking a trajectory in an analytical way. Though the proposed energy consumption function cannot be directly utilized in our work, the calculating ideas of the authors are still worth learning from.

A number of articles have concentrated on control algorithms directly designed for variable-pitch quadrotors and their flying strategies. Sheng et al. [15] suggested that variable-pitch quadrotors should be controlled based on the minimum power consumption principle, focusing less on the smoothness of control variables such as motor speeds and sometimes leading quadrotors to unhealthy flight behaviors. Jan et al. [16] proposed a

model-based controller designed for variable-pitch propellers, whose pitch angles minimized power consumption within the electric propulsion system for the given thrust value instead of optimizing rotation speeds and pitch angles at the same time. Gupta et al. [17] designed a model-based nonlinear controller for variable-pitch quadrotors, which might request larger computation resources, causing immediate changes in control variables. Moreover, the flexibility of pitch angle control was not utilized because the authors still implemented the control allocation module with only four variables. Similarly, Bo et al. [18] designed a nonlinear robust attitude controller using variable-pitch propellers as the propulsion system, but the control variables including rotation speeds and pitch angles were computed by forces with one-to-one correspondence, thus failing to utilize these variables in a satisfying manner. Additionally, the control system was designed based on a linear model with transfer-function-based controller design methods, causing negative effects to the robustness of the aircraft. In conclusion, though plenty of research has been conducted regarding variable-pitch propellers on various kinds of platforms, problems related to the control issues during the VTOL phase of large-scale eVTOLs still exist. Most controllers failed to sufficiently exploit the control potential of all eight control variables, and normally could not meet the specific application scenarios of large-scale VTOLs.

The purpose of this study is, therefore, to design and control a set of variable-pitch propellers for a typical electric VTOL (eVTOL) platform in order to track various kinds of trajectories under considerable external disturbances and measurement noise during the VTOL phase. Meanwhile, the power consumption of all propellers should be considered in case of exceeding the rated power. Detailed contributions are listed below.

- A typical tail-sitter eVTOL platform with distributed variable-pitch propellers is designed, which is able to achieve excellent flying performances during both the VTOL and cruise phase. Simulation data of the platform are then utilized as the objective for the designed controller with nonlinear flight dynamics. In addition, an actuator system consisting of four variable-pitch propellers is designed and its thrust and torque models are accurately analyzed.
- A specific optimization-based control allocation module is achieved to fully excavate the control potential of the variable-pitch propellers with four extra control variables, and the control allocation solution can be generated with low-dimensional quadratic programming solvers.
- This module is then mounted in a complete control system including position and attitude controllers to track the given trajectory. Constraints such as power consumption and the maximum rate of the control variables are considered to maintain the stability of the system.
- A series of simulation experiments are accomplished in order to validate the effectiveness of the designed controller under different circumstances, such as set-point arrival and aggressive trajectory tracking under measurement noise and external disturbances.

The structure of this paper is as follows: First, the platform design and analysis work for both the eVTOL and the variable-pitch propellers system, including flight dynamics interpretation, are addressed in Section 2. Then, the control and optimization strategies for the eVTOL utilizing the variable-pitch propeller system as the actuator are developed in Section 3, followed by simulation experiments and the results in Section 4. Finally, conclusions are drawn in Section 5.

## 2. System Design and Flight Dynamics Analysis

This section introduces the design and modeling of the eVTOL platform and the variable-pitch propeller system. For further convenience, the designed eVTOL platform and the related coordinate system definition are firstly introduced in Section 2.1. Then, the design and analysis work of a variable-pitch propeller system is explained in Section 2.2, followed by the dynamic model of the platform and the differential flatness property in Section 2.3.

2.1. Platform Introduction and Frame Description

The prototype eVTOL designed for this study is depicted in Figure 1, with a 120 kg maximum take-off mass. Since the eVTOL is designed for reconnaissance missions like inspection and observation, 10 kg of maximum payload mass is enough for installing photoelectric loads like visible light cameras. From the mechanical perspective, the maximum payload mass is able to reach 30 kg after adjusting the installation manners of batteries. Its cruise speed is planned as 34 m/s with a 60 m/s maximum speed with a high lift-to-drag ratio model and canard configuration, promoted by four distributed electric variable-pitch propellers. This eVTOL model serves as an excellent technological validation platform, combining the advantages of a high flight speed and extended flight range, and is utilized because its characteristics are closely related to our research objectives. Specifically, it is attributed to a typical tail-sitter eVTOL aircraft due to its structure, and is able to accomplish a series of 50 km long-distance flights owing to its sophisticated aerodynamic configurations. Its mission profile is shown in Figure 2. In this research, the VTOL phase flight is mainly discussed, so unnecessary details concerning the cruise phase including the transition phase of the aircraft will be appropriately abbreviated.

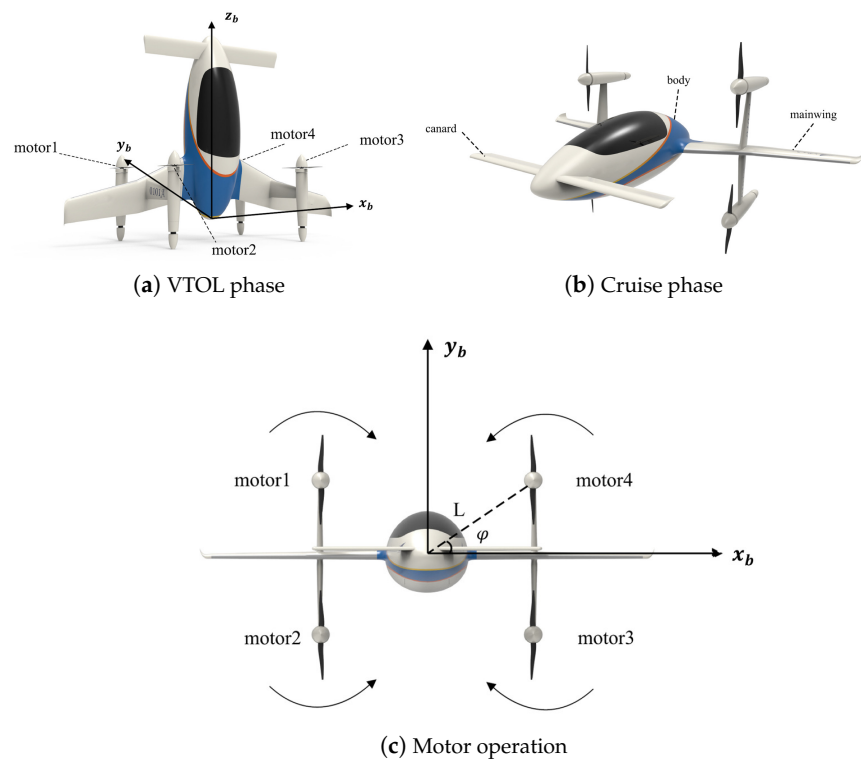


Figure 1. Appearances of the eVTOL and motors.

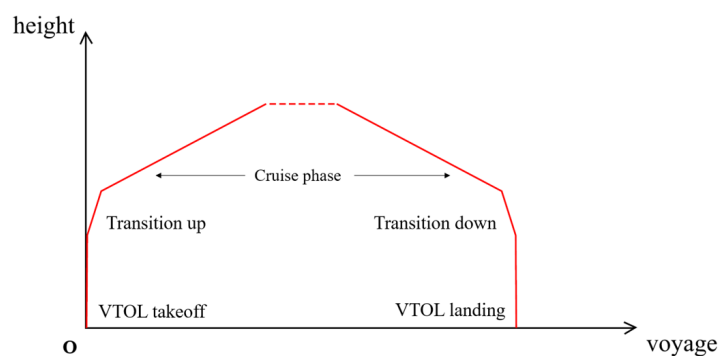


Figure 2. Flying phases of the eVTOL.

As shown in Figure 1, the definition of coordinate frames follows the convention of traditional quadrotors, and the relative positional relationship between the four propellers and the eVTOL platform is also depicted to explain the propeller system in latter chapters. The world frame  $\{O, x, y, z\}$  denoting East, North, Up (ENU) coordinates is considered as the inertial frame, and the body frame  $\{O_b, x_b, y_b, z_b\}$  is recognized as the body frame, where  $Oxz$  and  $Oyz$  are both symmetrical planes of the four propellers.

## 2.2. Variable-Pitch Propeller Design and Analysis

### 2.2.1. Propeller System Design

For the purpose of overcoming difficulties in that traditional propellers fail to provide sufficient thrust for large-scale eVTOL aircraft, a novel system of variable-pitch propellers is designed whose abilities are proven to be efficient for the power system demands of large-scale eVTOLs. Its aerodynamic appearance depicted in Figure 3 takes propeller blades NACA5868-9 as a reference, and its structure is modified after taking the wingtip effect and edge effect during real flight into consideration. The rotation speed and pitch angle control can be realized using the electric driving technique, with the propulsion system using Field-Oriented Control (FOC); thus, its pitch angle changing rate can reach  $30^\circ/\text{s}$  and its pitch angle can reach  $\pm 60^\circ$ . Specifically, the pitch angle is controlled using a position closed-loop system, making its measurement error less than  $1'$ .

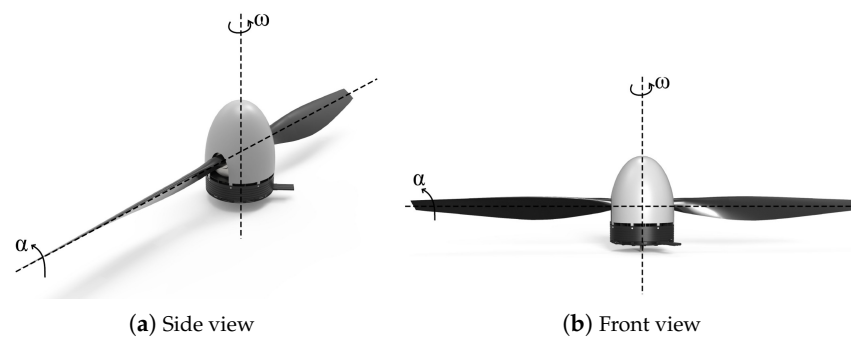


**Figure 3.** Propeller's aerodynamic appearance.

### 2.2.2. Efficiency Analysis

We compare the performances of the newly designed variable-pitch propellers and regular T-motor propellers during both the VTOL phase and the cruise phase, where the airspeeds of each phase are 0 and 30 m/s, respectively. Since the horizontal and vertical airspeeds are relatively low during the VTOL phase, which may cause numerical invalidation of the definition of the power efficiency, the force efficiency is recognized as the dependent variable, which is described in Equation (1).

$$\eta_F = \frac{\text{thrust}/g}{10^3 \cdot P} \quad (1)$$

where  $g$  is considered the gravitational acceleration,  $P$  is the overall power of the propeller, and the dimension of the force efficiency variable is  $g/W$ . As for flying circumstances during the cruise phase, the power efficiency is considered the dependent variable as usual. Additionally, for the independent variables, forward ratio is frequently recognized as the variable to describe the flying states during the normal cruise phase of the aircraft, as shown in Equation (2), where  $\omega$  refers to the rotation speed and  $D$  refers to the diameter of the propeller.

$$J_{\text{forward}} = \frac{\text{airspeed}}{\omega D} \quad (2)$$

However, since the airspeed is approximately zero during the VTOL phase, rotation speeds are regarded as the dependent variable due to their determinant effect on the flight

status. Both of the efficiency simulation results during the different phases are shown in Figure 4 with original data points simulated in CFD software (Available online: <https://www.simscale.com/product/cfd/>, accessed on 22 March 2024), and fitted through least-squares methods during the VTOL phase or interpolation through cubic splines during the cruise phase.

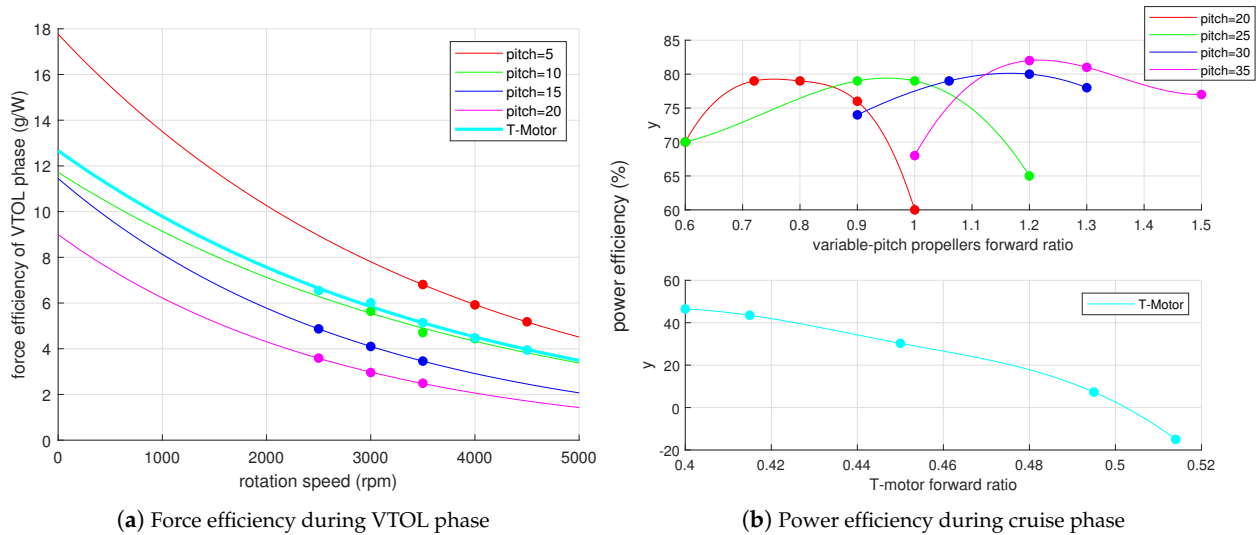


**Figure 4.** Efficiency analysis of both flying phases.

Some conclusions can be indicated according to the simulation results. First, both propeller systems work well during the VTOL phase, while the variable-pitch propeller system performs much better during the cruise phase. Specifically, when the airspeed reaches about 30 m/s during the cruise phase, the T-motor system just starts to have positive efficiency with an approximately 3600 rpm rotation speed, and finally achieves 46% efficiency with 4500 rpm, which is nearly the highest rotation speed of the motor. However, under the effects of relatively large pitch angles during the cruise phase, the variable-pitch propeller system is able to maintain 80% efficiency even if the rotation speed is at normal.

Focusing on the results of the variable-pitch propeller system during the VTOL phase, it can be seen that the force efficiency undergoes significant downward gliding as the pitch angle increases, indicating that the pitch angle should be constrained at a low level during this phase. As a result, when conducting simulation experiments to verify the influence of pitch angle control in Section 4, the fixed pitch angle might as well be set at relatively low values such as  $5^\circ$  or  $10^\circ$ .

In short, analysis on both the force efficiency during the VTOL phase and the power efficiency during the cruise phase suggests that if the control variables such as pitch angles and rotation speeds are validly controlled, the designed variable-pitch propeller system is able to work fantastically during both phases, while the regular propeller system is exposed as having certain shortcomings, especially during the cruise phase.

### 2.2.3. Propulsion System Model Analysis

After validating the efficiency of the variable-pitch propeller system during both phases, its functionality as the propulsion system model of the eVTOL aircraft is next to be defined. This is normally described as the relationship between the inputs, which are the airspeed, propeller pitch angle, and rotation speed, and the outputs, which are the force and torque provided by each propeller. Since this paper concentrates on control system design during the VTOL phase, the airspeed can be temporarily neglected as it is approximately zero all of the time. Earlier research [19] revealed that under this situation,



as for one propeller, the combination of its rotational speed  $\omega$  and pitch angle  $\alpha$  produces the lift force  $F$  in the direction of the propeller axis as in Equation (3).

$$F_i = (k_{F1}\alpha_i + k_{F2})\omega_i^2, \quad i = 1, 2, 3, 4 \tag{3}$$

where  $k_{F1}$  and  $k_{F2}$  are two motor constants whose estimations can be acquired through data points from CFD simulation and least-squares regression. Similarly, the drag moment produced by one propeller can then be formulated as Equation (4) [10,19]:

$$M_i = k_{M1}\omega_i^2\alpha_i^2 + k_{M2}\omega_i^2 + k_{M3}\alpha_i\omega_i, \quad i = 1, 2, 3, 4 \tag{4}$$

where  $k_{M1}$ ,  $k_{M2}$ , and  $k_{M3}$  can also be considered as motor constants. The approximation figures are exhibited in Figure 5, and the obtained parameters, which are listed in the parameter table in Table 1, will be recognized as the actuator model.

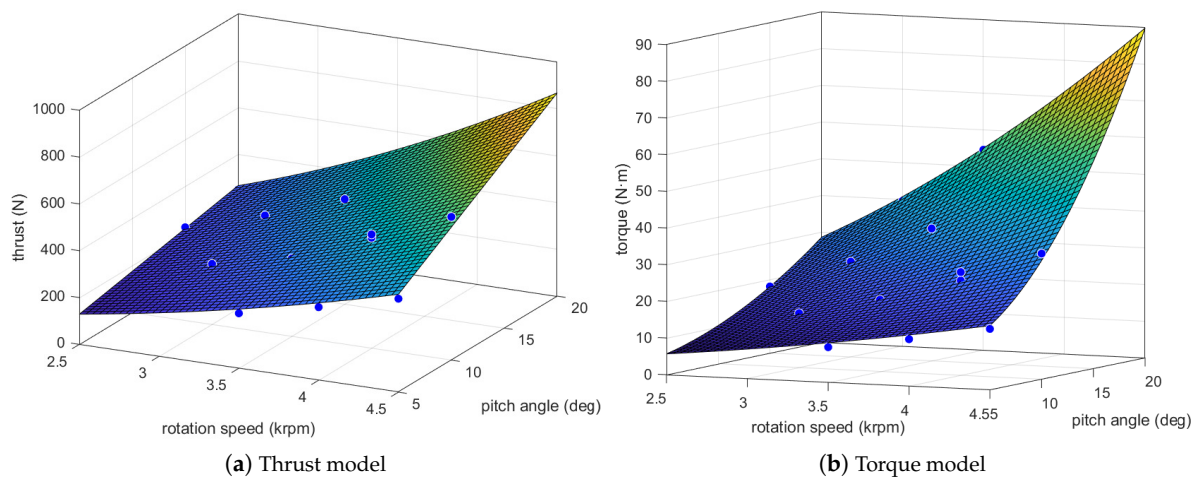


Figure 5. Aerodynamic models of a variable-pitch propeller.

Table 1. Parameter table.

Parameter	Value	Notation
$g$	$9.76 \text{ [m/s}^2\text{]}$	gravitational acceleration
$I$	$diag(76.9, 82.3, 128.8) \text{ [kg} \cdot \text{m}^2\text{]}$	moment of inertia
$k_{F1}$	1.482	motor parameters
$k_{F2}$	13.23	
$k_{M1}$	$9.158 \times 10^{-3}$	
$k_{M2}$	0.5933	
$k_{M3}$	$4.147 \times 10^{-2}$	
$K_\alpha$	$I_{4 \times 4}$	optimization coefficients
$K_\omega$	$20 \cdot I_{4 \times 4}$	
$K_u$	$50,000 \cdot I_{4 \times 4}$	
$K_p$	$50,000 \cdot I_{4 \times 4}$	
$L$	$[2.5, 1.5] \text{ [m]}$	motor installation position
$\varphi$	$30.9 \text{ [deg]}$	motor installation angle
$m$	$101.8 \text{ [kg]}$	eVTOL mass
$P_{max}$	$10 \text{ [kW]}$	maximum power
$\omega_{max}$	$4500 \text{ [rpm]}$	maximum rotation speed
$\dot{\omega}_{max}$	$800 \text{ [rpm/s]}$	maximum rotation acceleration
$\alpha_{max}$	$25 \text{ [deg]}$	maximum pitch angle
$\alpha_{min}$	$-15 \text{ [deg]}$	minimum pitch angle
$\dot{\alpha}_{max}$	$30 \text{ [deg/s]}$	maximum pitch velocity

### 2.3. Aircraft Dynamics and Differential Flatness Property

A 12-dimensional vector including position, orientation, linear velocity, and angular velocity is considered as the eVTOL's state vector as follows [20]

$$\mathbf{X} = [x, y, z, \phi, \theta, \psi, \dot{x}, \dot{y}, \dot{z}, \omega_x, \omega_y, \omega_z]^T \quad (5)$$

Under the circumstance of low-speed flight ( $\|v\| < 10$  m/s) during the VTOL phase, the aerodynamic factors have little impact on the overall dynamics of the aircraft, which means the model receives its force and torque only from gravity and the four variable-pitch propellers. Therefore, the Newton equation and Euler equation can be given as

$$m\ddot{\mathbf{p}} = \begin{bmatrix} 0 \\ 0 \\ -mg \end{bmatrix} + \mathbf{R} \begin{bmatrix} 0 \\ 0 \\ F_1 + F_2 + F_3 + F_4 \end{bmatrix} \quad (6)$$

$$\mathbf{J}_M \cdot \begin{bmatrix} \dot{\omega}_x \\ \dot{\omega}_y \\ \dot{\omega}_z \end{bmatrix} + \begin{bmatrix} \omega_x \\ \omega_y \\ \omega_z \end{bmatrix} \times \mathbf{J}_M \cdot \begin{bmatrix} \omega_x \\ \omega_y \\ \omega_z \end{bmatrix} = \begin{bmatrix} L \cos \varphi (F_1 - F_2 - F_3 + F_4) \\ L \sin \varphi (F_1 + F_2 - F_3 - F_4) \\ M_1 - M_2 + M_3 - M_4 \end{bmatrix}$$

in which  $\mathbf{R}$  represents the rotation matrix from the eVTOL model body frame to the world frame. Given the eVTOL's state vector measured by corresponding sensors,  $\mathbf{R}$  can be defined as Equation (7) with the rotation order of Z-Y-X.

$$\mathbf{R} = \mathbf{R}_\psi \mathbf{R}_\theta \mathbf{R}_\phi = \begin{bmatrix} c\psi c\theta & c\psi s\theta s\phi - s\psi c\phi & c\psi s\theta c\phi + s\psi s\theta \\ s\psi c\theta & s\psi s\theta s\phi + c\psi c\phi & s\psi s\theta c\phi - c\psi s\theta \\ -s\theta & c\theta s\phi & c\theta c\phi \end{bmatrix} \quad (7)$$

Additionally,  $\mathbf{J}_M$  represents the moment of inertia of the eVTOL platform, and for the parameters of the motors,  $L$  indicates the distance between the motor and the centroid of the eVTOL, and  $\varphi$  indicates the respective angle. Positional relationships among the four installed motors are shown in Figure 1.

To enable automated generation of trajectories and control, a differential flatness property [21] is raised, which means that the states and the inputs of the eVTOL aircraft can be written as algebraic functions of four carefully selected flat outputs and their derivatives, in this case,  $\sigma = [x, y, z, \psi]$ . Therefore, the trajectory generation module only needs to provide four flat output curves over time, which can be utilized by the controller system to generate eight control variables for the eVTOL objective.

## 3. Control Law Design

After presenting the coordinate system, vehicle construction as well as the power system, this section focuses on the control manners to effectively operate eight control variables including four rotation speeds and four pitch angles. Since the main characteristics of the variable-pitch propeller take place in the redundancy of control variables, the design and analysis of the control allocation module are emphasized. The overview of the designed controller system is illustrated in Section 3.1, followed by the penalty function construction of the optimization problem in Section 3.2. Finally, the way to generate eight control variables directly from the control outputs of these controllers will be explained in Section 3.3.

### 3.1. Control System Overview

The control architecture as a whole is summarized in Figure 6. First, the trajectory generation module provides a smooth trajectory with timestamps, which includes  $x(t)$ ,  $y(t)$ ,  $z(t)$ , and  $\psi(t)$ , and then other parameters can be calculated based on the differential flatness property. This trajectory can be generated by positioning curves such as straight lines and sine waves, or by classical trajectory generation techniques like minimum snap [21] or EGO-Planner [22].



Next, the position controller module makes use of this trajectory, combined with the information returned from the sensors of the eVTOL model, in order to generate a series of roll and pitch angles for the attitude controller with a cascade PID structure. The first control element  $u_1$  is also generated, which relies only on the position control variables. Then, the attitude controller module receives references provided by the position controller as well as the trajectory generation module and generates three attitude-related control elements  $u_2, u_3, u_4$  with a similar cascade PID structure. Up to this point, based on the trajectory planner and controllers, the four control elements are all provided, which is described in Equation (8).

$$u_1 = \left\| m \begin{bmatrix} a_x \\ a_y \\ a_z + g \end{bmatrix} \right\| \tag{8}$$

$$\begin{bmatrix} u_2 \\ u_3 \\ u_4 \end{bmatrix} = \mathbf{J}_M \cdot \begin{bmatrix} \dot{\omega}_x \\ \dot{\omega}_y \\ \dot{\omega}_z \end{bmatrix} + \begin{bmatrix} \omega_x \\ \omega_y \\ \omega_z \end{bmatrix} \times \mathbf{J}_M \cdot \begin{bmatrix} \omega_x \\ \omega_y \\ \omega_z \end{bmatrix}$$

Finally, these four elements are passed to the control allocation module, which plays an important role, especially when using the variable-pitch propeller system as the actuator. Eight control variables are provided to deal with only four control inputs, offering a huge amount of free space for this module to achieve better characteristics than normal quadrotors. After the control allocation module, four motor speeds along with four propeller angles are given to the eVTOL model, enabling it to successfully track the ideal trajectory and achieve satisfying flight performance as well as minimizing energy consumption at the same time.

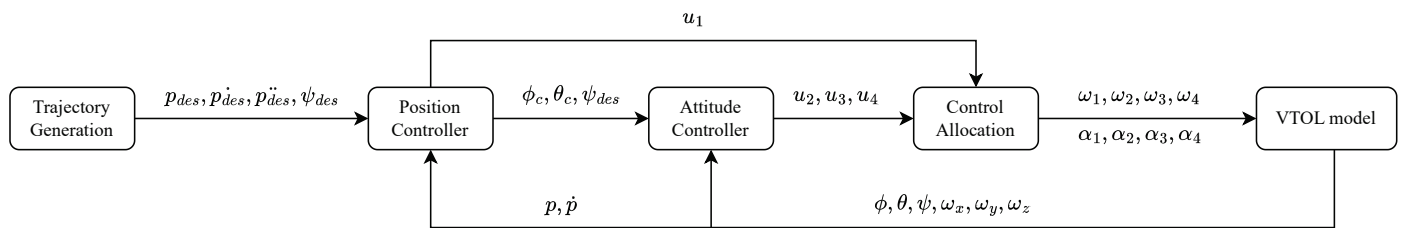


Figure 6. Control system overview.

### 3.2. Penalty Function Construction

Three penalty functions are designed to guarantee a high-quality flight; specifically, the accuracy, stability, and low energy consumption of the flight during the VTOL phase should be realized simultaneously.

#### 3.2.1. Control Inputs' Penalty

According to the aircraft dynamics explained in Section 2.3, the four control inputs can all be represented by eight control outputs including four rotational speeds and four propeller pitches as

$$\begin{aligned} u_1 &= F_1 + F_2 + F_3 + F_4 \\ u_2 &= L \cos \varphi (F_1 - F_2 - F_3 + F_4) \\ u_3 &= L \sin \varphi (F_1 + F_2 - F_3 - F_4) \\ u_4 &= -M_1 + M_2 - M_3 + M_4 \end{aligned} \tag{9}$$

For the control allocation module, it is required to minimize the error between the recently received control input vector

$$\overline{\mathbf{u}}_{\text{now}} = \left[ \overline{f}_{\text{total}}, \overline{\tau}_{\text{roll}}, \overline{\tau}_{\text{pitch}}, \overline{\tau}_{\text{yaw}} \right]^T \tag{10}$$

and the control input vector that could be provided by eight control outputs

$$\overline{\mathbf{u}}_{\text{change}} = [u_1(\boldsymbol{\alpha}, \boldsymbol{\omega}), u_2(\boldsymbol{\alpha}, \boldsymbol{\omega}), u_3(\boldsymbol{\alpha}, \boldsymbol{\omega}), u_4(\boldsymbol{\alpha}, \boldsymbol{\omega})]^T \quad (11)$$

in which  $\boldsymbol{\alpha} = [\alpha_1, \alpha_2, \alpha_3, \alpha_4]^T$  and  $\boldsymbol{\omega} = [\omega_1, \omega_2, \omega_3, \omega_4]^T$ . In the hope of tracking the given trajectory in time, the control input provided by rotation speeds and pitch angles,  $\overline{\mathbf{u}}_{\text{change}}$ , should make an effort to approach closer to the recently received control input,  $\overline{\mathbf{u}}_{\text{now}}$ ; thus, the distinction between these two control inputs  $\overline{\mathbf{u}}_{\text{change}}$  and  $\overline{\mathbf{u}}_{\text{now}}$  must be significantly reflected in the objective function. As a result, the control inputs' penalty term can be written as

$$\mathbf{J}_{\mathbf{u}} = \mathbf{K}_{\mathbf{u}} \left\| \overline{\mathbf{u}}_{\text{now}} - \overline{\mathbf{u}}_{\text{change}} \right\|^2 \quad (12)$$

### 3.2.2. Control Variables' Shifting Penalty

Since there are eight controllable outputs determining the control input vector  $\mathbf{u}$  consisting of four control inputs, there are endless solutions to allocate these outputs just to track the given trajectory. However, if the control allocation module casually chooses one of these solutions at a time, the response of the rotation speeds and pitch angles might be so chaotic that real-world hardware equipment can barely keep pace with them. Moreover, since the changing abilities of pitch angles are much better than those of rotation speeds, and make rotation speeds change to a slower rate, which is good for the persistent maintenance of the motors' performance, the shifting of rotation speeds should be given more of a penalty. Therefore, the change in the eight control variables should be restricted by both the objective function and constraints in case sudden motor speed changes occur, and the change in rotation speeds should be more strictly constrained. In conclusion, the control variables' shifting penalty term can be listed as

$$\mathbf{J}_{\mathbf{s}} = \mathbf{K}_{\boldsymbol{\alpha}} \left\| \boldsymbol{\alpha} - \boldsymbol{\alpha}_{\text{last}} \right\|^2 + \mathbf{K}_{\boldsymbol{\omega}} \left\| \boldsymbol{\omega} - \boldsymbol{\omega}_{\text{last}} \right\|^2 \quad (13)$$

where  $\mathbf{K}_{\boldsymbol{\omega}} > \mathbf{K}_{\boldsymbol{\alpha}}$  significantly.

### 3.2.3. Energy Consumption Penalty

What is more, despite the high functionality such as the sufficient forces and torques provided by variable-pitch propellers, they can cause huge energy loss if the control variables are arranged inappropriately. Therefore, it is necessary to optimize the control variables with energy consumption fully considered. The mechanical power of the propellers is considered, which can be given as

$$P_i = M_i \omega_i = \left( k_{M1} \omega_i^2 \alpha_i^2 + k_{M2} \omega_i^2 + k_{M3} \alpha_i \omega_i \right) \omega_i, \quad i = 1, 2, 3, 4 \quad (14)$$

where for propeller  $i$ ,  $M_i$  is the torque described in Equation (4), and thus  $P_i$  depends and only depends on the rotation speed  $\omega_i$  and the pitch angle  $\alpha_i$ . Contour lines of power  $P_i$  with respect to  $\omega_i$  and  $\alpha_i$  are shown in Figure 7. As discussed in Section 2.2, the mechanical power of each propeller must be constrained below the rated power, which is approximately 12 kW in bold in Figure 7, in case of overheating inside the propellers. In this research, it is further restricted under 10 kW to protect the propellers from damage in case of sudden accidents, which is also in bold in Figure 7. Control variables must be carefully calculated with limiting power consumption as a high priority, whose penalty function can be represented as

$$\mathbf{J}_{\mathbf{P}} = \mathbf{K}_{\mathbf{p}} \left\| \mathbf{P} \right\|^2 \quad (15)$$

These factors should all be considered during the process of constructing the optimization objective of the control allocation module, whose form directly determines the effectiveness and feasibility of the whole optimization problem.

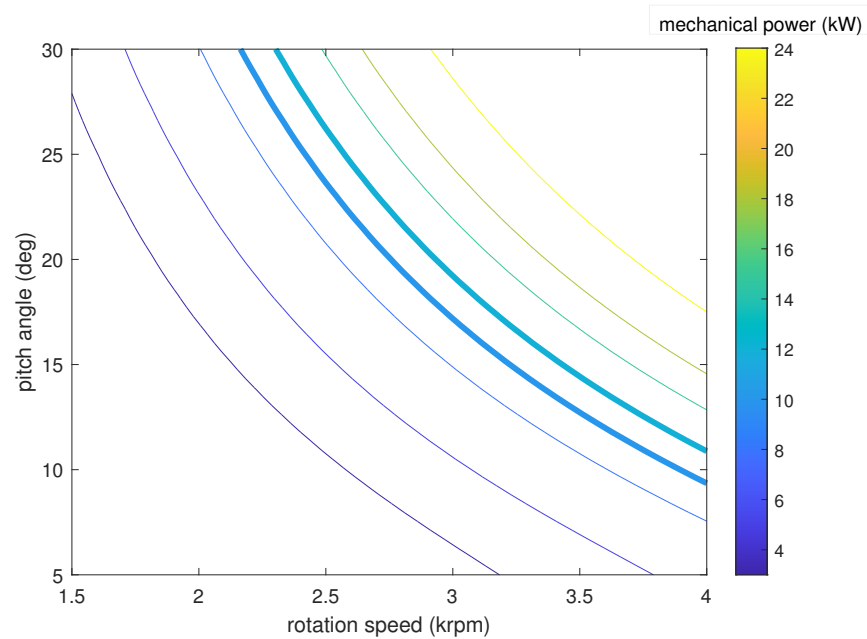


Figure 7. Mechanical power contour curves.

### 3.3. Optimization-Based Control Allocation Algorithm

Different from traditional propellers whose force and torque are proportional to the square of rotational speeds, as for variable-pitch propellers, not only force and torque are dependent on both rotational speed and propeller pitch, but these formulas consist of various kinds of polynomials, making it difficult to construct and solve the related control allocation problem. If eight control outputs are directly appointed as optimization variables, the optimization formula will be set as

$$\min_{\alpha, \omega} \mathbf{K}_u \|\overline{\mathbf{u}}_{\text{now}} - \overline{\mathbf{u}}_{\text{change}}\|^2 + \mathbf{K}_\alpha \|\alpha - \alpha_{\text{last}}\|^2 + \mathbf{K}_\omega \|\omega - \omega_{\text{last}}\|^2 + \mathbf{K}_p \|\mathbf{P}\|^2 \quad (16)$$

s.t.

$$\alpha \in [\alpha_{\min}, \alpha_{\max}] \quad (16a)$$

$$\omega \in [\omega_{\min}, \omega_{\max}] \quad (16b)$$

$$\alpha - \alpha_{\text{last}} \in [-\dot{\alpha}_{\max}, \dot{\alpha}_{\max}] \Delta t \quad (16c)$$

$$\omega - \omega_{\text{last}} \in [-\dot{\omega}_{\max}, \dot{\omega}_{\max}] \Delta t \quad (16d)$$

$$P_i \in [\mathbf{0}_{4 \times 1}, P_{\max} \cdot \mathbf{1}_{4 \times 1}], \quad i = 1, 2, 3, 4 \quad (16e)$$

in which  $\alpha_{\text{last}}$  and  $\omega_{\text{last}}$  are control variables that were generated from the control allocation module at the last step, and  $\mathbf{0}_{4 \times 1}$ ,  $\mathbf{1}_{4 \times 1}$  indicate two  $4 \times 1$  vectors full of zeros and ones, respectively. It is somehow straightforward to recognize that the optimization function contains at most the sixth order of  $\omega$  as well as the fourth order of  $\alpha$ , which is a combination of tenth order, making the optimization problem extremely hard to solve. Some numerical optimization methods like PHR-ALM [23] are able to deal with general objective functions with linear constraints; however, the solving efficiency is not able to meet the requirements of the control allocation module, and numerical instability frequently occurs under this high-order circumstance.

Fortunately, the most recent control variables,  $\alpha_{\text{last}}$  and  $\omega_{\text{last}}$ , could be acquired from sensors in time. Consequently, instead of insisting on this hard optimization formula where  $\alpha$  and  $\omega$  are considered as optimization variables, the control allocation module chooses their variations  $\Delta\alpha$  and  $\Delta\omega$ , then utilizes first-order approximation to realize reliable optimization effects as well as significantly decrease the difficulty of solving the formula.

The new optimization problem whose control variables are listed as  $\Delta\alpha$  and  $\Delta\omega$  is then constructed as follows

$$\min_{\Delta\alpha, \Delta\omega} \mathbf{K}_u \left\| \bar{\mathbf{u}}_{\text{now}} - \left( \bar{\mathbf{u}}_{\text{last}} + \frac{\partial \bar{\mathbf{u}}_{\text{change}}}{\partial \alpha} \Delta\alpha + \frac{\partial \bar{\mathbf{u}}_{\text{change}}}{\partial \omega} \Delta\omega \right) \right\|^2 + \mathbf{K}_\alpha \|\Delta\alpha\|^2 + \mathbf{K}_\omega \|\Delta\omega\|^2 + \mathbf{K}_p \left\| \mathbf{P}_{\text{last}} + \frac{\partial \mathbf{P}}{\partial \alpha} \Delta\alpha + \frac{\partial \mathbf{P}}{\partial \omega} \Delta\omega \right\|^2 \quad (17)$$

s.t.

$$\Delta\alpha \in [(\alpha_{\min} - \alpha_{\text{last}}) \cdot \mathbf{1}_{4 \times 1}, (\alpha_{\max} - \alpha_{\text{last}}) \cdot \mathbf{1}_{4 \times 1}] \quad (17a)$$

$$\Delta\omega \in [(\omega_{\min} - \omega_{\text{last}}) \cdot \mathbf{1}_{4 \times 1}, (\omega_{\max} - \omega_{\text{last}}) \cdot \mathbf{1}_{4 \times 1}] \quad (17b)$$

$$\Delta\alpha \in [-\alpha_{\max} \cdot \mathbf{1}_{4 \times 1}, \alpha_{\max} \cdot \mathbf{1}_{4 \times 1}] \Delta t \quad (17c)$$

$$\Delta\omega \in [-\omega_{\max} \cdot \mathbf{1}_{4 \times 1}, \omega_{\max} \cdot \mathbf{1}_{4 \times 1}] \Delta t \quad (17d)$$

$$\Delta\mathbf{p} = \frac{\partial \mathbf{P}}{\partial \alpha} \Delta\alpha + \frac{\partial \mathbf{P}}{\partial \omega} \Delta\omega \leq \mathbf{P}_{\max} - \mathbf{P}_{\text{last}} \quad (17e)$$

where partial derivatives in the Problem can be calculated as

$$\begin{aligned} \mathbf{U}_\alpha &\triangleq \frac{\partial \bar{\mathbf{u}}_{\text{change}}}{\partial \alpha} = \left[ \frac{\partial u_1}{\partial \alpha}, \frac{\partial u_2}{\partial \alpha}, \frac{\partial u_3}{\partial \alpha}, \frac{\partial u_4}{\partial \alpha} \right]^T \\ \mathbf{U}_\omega &\triangleq \frac{\partial \bar{\mathbf{u}}_{\text{change}}}{\partial \omega} = \left[ \frac{\partial u_1}{\partial \omega}, \frac{\partial u_2}{\partial \omega}, \frac{\partial u_3}{\partial \omega}, \frac{\partial u_4}{\partial \omega} \right]^T \\ \mathbf{P}_\alpha &\triangleq \frac{\partial \mathbf{P}}{\partial \alpha} = \left[ \frac{\partial P_1}{\partial \alpha}, \frac{\partial P_2}{\partial \alpha}, \frac{\partial P_3}{\partial \alpha}, \frac{\partial P_4}{\partial \alpha} \right]^T \\ \mathbf{P}_\omega &\triangleq \frac{\partial \mathbf{P}}{\partial \omega} = \left[ \frac{\partial P_1}{\partial \omega}, \frac{\partial P_2}{\partial \omega}, \frac{\partial P_3}{\partial \omega}, \frac{\partial P_4}{\partial \omega} \right]^T \end{aligned} \quad (18)$$

Given Equations (3), (4) and (9), the partial derivatives with respect to  $\alpha$  can be computed as

$$\begin{aligned} \frac{\partial u_1}{\partial \alpha} &= k_{F1} [\omega_1^2, \omega_2^2, \omega_3^2, \omega_4^2] \\ \frac{\partial u_2}{\partial \alpha} &= k_{F1} L \cos \varphi [\omega_1^2, -\omega_2^2, -\omega_3^2, \omega_4^2] \\ \frac{\partial u_3}{\partial \alpha} &= k_{F1} L \sin \varphi [\omega_1^2, \omega_2^2, -\omega_3^2, -\omega_4^2] \\ \frac{\partial u_4}{\partial \alpha} &= 2k_{M1} [-\alpha_1 \omega_1^2, \alpha_2 \omega_2^2, -\alpha_3 \omega_3^2, \alpha_4 \omega_4^2] + k_{M3} [-\omega_1, \omega_2, -\omega_3, \omega_4] \end{aligned} \quad (19)$$

Similarly, the partial derivatives with respect to  $\omega$  can be calculated as

$$\begin{aligned} \frac{\partial u_1}{\partial \omega} &= 2k_{F1} [\alpha_1 \omega_1, \alpha_2 \omega_2, \alpha_3 \omega_3, \alpha_4 \omega_4] + 2k_{F2} [\omega_1, \omega_2, \omega_3, \omega_4] \\ \frac{\partial u_2}{\partial \omega} &= 2k_{F1} L \cos \varphi [\alpha_1 \omega_1, -\alpha_2 \omega_2, -\alpha_3 \omega_3, \alpha_4 \omega_4] + 2k_{F2} L \cos \varphi [\omega_1, -\omega_2, -\omega_3, \omega_4] \\ \frac{\partial u_3}{\partial \omega} &= 2k_{F1} L \sin \varphi [\alpha_1 \omega_1, \alpha_2 \omega_2, -\alpha_3 \omega_3, -\alpha_4 \omega_4] + 2k_{F2} L \sin \varphi [\omega_1, \omega_2, -\omega_3, -\omega_4] \\ \frac{\partial u_4}{\partial \omega} &= 2k_{M1} [-\alpha_1^2 \omega_1, \alpha_2^2 \omega_2, -\alpha_3^2 \omega_3, \alpha_4^2 \omega_4] + 2k_{M2} [-\omega_1, \omega_2, -\omega_3, \omega_4] + k_{M3} [-\alpha_1, \alpha_2, -\alpha_3, \alpha_4] \end{aligned} \quad (20)$$

Different from the four control inputs, which are almost related to all eight control outputs, the power function of each propeller is dependent on only its rotation speed and pitch angle, as described in Equation (14). Therefore, the partial derivatives of power vector  $\mathbf{P}$  with respect to the rotation speed vector  $\boldsymbol{\omega}$  and pitch angle vector  $\boldsymbol{\alpha}$  are both diagonal matrices, which can be written as

$$\begin{aligned} \mathbf{P}_\alpha &= \text{diag}(2k_{M1}\alpha_1\omega_1^3 + k_{M3}\omega_1^2, 2k_{M1}\alpha_2\omega_2^3 + k_{M3}\omega_2^2, \\ &\quad 2k_{M1}\alpha_3\omega_3^3 + k_{M3}\omega_3^2, 2k_{M1}\alpha_4\omega_4^3 + k_{M3}\omega_4^2) \\ \mathbf{P}_\omega &= \text{diag}(3k_{M1}\alpha_1^2\omega_1^2 + 3k_{M2}\omega_1^2 + 2k_{M3}\alpha_1\omega_1, 3k_{M1}\alpha_2^2\omega_2^2 + 3k_{M2}\omega_2^2 + 2k_{M3}\alpha_2\omega_2, \\ &\quad 3k_{M1}\alpha_3^2\omega_3^2 + 3k_{M2}\omega_3^2 + 2k_{M3}\alpha_3\omega_3, 3k_{M1}\alpha_4^2\omega_4^2 + 3k_{M2}\omega_4^2 + 2k_{M3}\alpha_4\omega_4) \end{aligned} \quad (21)$$

At this point, the basic framework of the control allocation module has been completed. With the intention of simplifying the problem and revealing its fundamental structure, the definitions are set as follows

$$\Delta \mathbf{x} \triangleq [\Delta \boldsymbol{\omega}^T, \Delta \boldsymbol{\alpha}^T]^T \in \mathbb{R}^{8 \times 1} \quad (22)$$

$$\Delta \mathbf{u}_{\text{real}} \triangleq \overline{\mathbf{u}_{\text{now}}} - \overline{\mathbf{u}_{\text{last}}} \in \mathbb{R}^{4 \times 1} \quad (23)$$

$$\mathbf{U} \triangleq [\mathbf{U}_\omega, \mathbf{U}_\alpha] \in \mathbb{R}^{4 \times 8} \quad (24)$$

$$\mathbf{U}_P \triangleq [\mathbf{P}_\omega, \mathbf{P}_\alpha] \in \mathbb{R}^{4 \times 8} \quad (25)$$

$$\mathbf{K} \triangleq \begin{bmatrix} \mathbf{K}_\omega & \mathbf{0}_{4 \times 4} \\ \mathbf{0}_{4 \times 4} & \mathbf{K}_\alpha \end{bmatrix} \in \mathbb{R}^{8 \times 8} \quad (26)$$

With these definitions, the objective function  $J$  can be rewritten as

$$\begin{aligned} J &= \mathbf{K}_u \|\Delta \mathbf{u}_{\text{real}} - \mathbf{U} \Delta \mathbf{x}\|^2 + \mathbf{K} \|\Delta \mathbf{x}\|^2 + \mathbf{K}_p \|\mathbf{P}_{\text{last}} + \mathbf{U}_P \Delta \mathbf{x}\|^2 \\ &= \Delta \mathbf{x}^T \left( \mathbf{U}^T \mathbf{K}_u \mathbf{U} + \mathbf{K} + \mathbf{U}_P^T \mathbf{K}_p \mathbf{U}_P \right) \Delta \mathbf{x} - 2 \Delta \mathbf{u}_{\text{real}}^T \mathbf{K}_u \mathbf{U} \Delta \mathbf{x} + 2 \mathbf{P}_{\text{last}}^T \mathbf{K}_p \mathbf{U}_P \Delta \mathbf{x} + c \end{aligned} \quad (27)$$

where  $c$  is a constant that is unrelated to the optimization variable  $\Delta \mathbf{x}$ . Since the quadratic term of the objective function is constructed of the sum of forms  $\mathbf{A}^T \mathbf{K} \mathbf{A}$  and  $\mathbf{K}$  is a coefficient matrix, which is a positive definite diagonal matrix, the quadratic term can obviously be proven to be a semi-definite matrix. Moreover, since  $\mathbf{U}$  and  $\mathbf{U}_P$  have full row rank 4 when all of the rotation speeds are positive ( $\omega_i > 0$ ,  $i = 1, 2, 3, 4$ ), the quadratic term matrix can be confirmed as a strictly definite matrix, making the problem a strictly convex quadratic programming problem. What is more, owing to the fact that  $\Delta \mathbf{x}$  is only 8-dimensional, it can be treated as a low-dimensional QP problem with linear inequality constraints.

Plenty of QP solvers are able to solve this problem. However, since the control allocation module requires a relatively fast solving rate in order to keep pace with the commands of controllers in time, while highly accurate rotation speed and propeller pitch commands are also required, a solver called SDQP [24] is chosen, which is able to provide exact solutions with low  $O(d!n)$  complexity. In this case,  $d$  represents the dimension of the optimization variable, which is eight, and  $n$  means the number of constraints. Different from other solvers such as QP solvers in MATLAB, the SDQP solver provides an exact solution based on the low-dimensional circumstance of this specific QP with low complexity, which plays an irreplaceable role in the successful implementations of the controller.

To sum up, the control allocation module can be constructed based on actuator models, first-order approximation of the objective function, and the SDQP solver. The whole structure of the control allocation module is depicted in Figure 8. Along with other established controller modules, the overall control law for the eVTOL aircraft is completed.

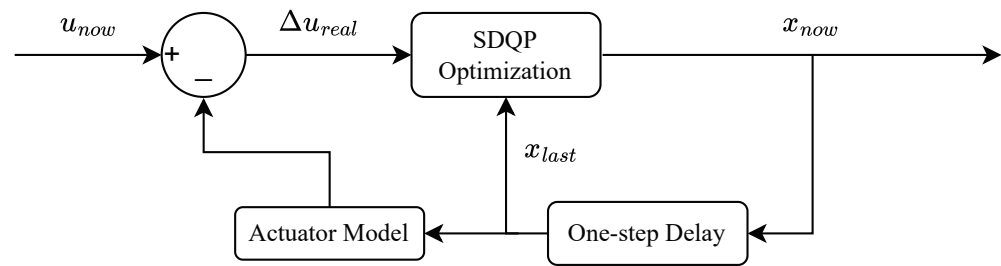


Figure 8. Control allocation module description.

#### 4. Simulation Experiments

This section presents three simulation scenarios to verify the effectiveness of the designed control law. The simulations are performed using Simulink in MATLAB, where the SDQP solver is able to solve the problem in less than 1 ms. Thanks to the conversion from the original high-level optimization problem to a low-dimensional structured QP problem, the efficiency of solving it improves dramatically. Therefore, the frequency of the positional controller is set as 50 Hz and the attitude controller as well as the control allocation module are set as 500 Hz. Additionally, all of these scenarios are conducted with the eVTOL model introduced in Section 2, and without loss of generality. When bringing up the comparison between variable-pitch propellers and regular ones, the simulation sets the motor parameters of the latter under the condition that pitch angle  $\alpha$  remains constant, normally at  $5^\circ$  or  $10^\circ$  since the force efficiency is too low for the aircraft to take off if  $\alpha$  gets any higher.

The first scenario suggests the effectiveness of the controller-given set-point control scene, the second scenario indicates its ability to track more aggressive trajectories, and the last scenario proves its robustness under noisy measurements and external disturbances.

The performance of the controller is validated in this section under different scenarios. The first scenario is about the set-point-arriving scene in Section 4.1, while the second scenario provides a much more complicated and aggressive trajectory in Section 4.2. Moreover, the third scenario concentrates more on measurement noises and external disturbances, as shown in Section 4.3. Finally, the numerical error analysis results are shown in Section 4.4. The parameter table is depicted in Table 1.

##### 4.1. Set-Point Control

One of the basic missions of any successfully designed controller is the set-point controlling task. It is worth mentioning that, throughout this section, the initial condition of the four variable-pitch propellers is set as

$$\begin{cases} \omega_i = \sqrt{\frac{mg}{4k_{M2}}}, & i = 1, 2, 3, 4 \\ \alpha_i = 0, & i = 1, 2, 3, 4 \end{cases} \quad (28)$$

For regular propeller conditions, the virtual “pitch angle” is kept at  $5^\circ$  or  $10^\circ$  constantly in order to verify the effectiveness of the designed controller. Consequently, the initial condition is set as

$$\omega_i = \sqrt{\frac{mg}{4(k_{M1}\alpha_{\text{set}} + k_{M2})}} \quad i = 1, 2, 3, 4 \quad (29)$$

The coordinates of the target point are denoted as

$$x = 0.5 \text{ m}, y = 0.4 \text{ m}, z = 1 \text{ m} \quad (30)$$

Even though the target point seems fairly close to the original, the relative distance is reasonable because consecutive intermediate points are calculated from the trajectory generation module instead of an extremely far target. The performance of the proposed controller is depicted in Figure 9. As is described in these results, the eVTOL aircraft arrives at the designated target point in about 6 s, with approximately 6.5 kW the highest power



and a power of 3.8 kW, ultimately, for each propeller. Therefore, the overall controlling performance of the variable-pitch propeller system is acceptable.

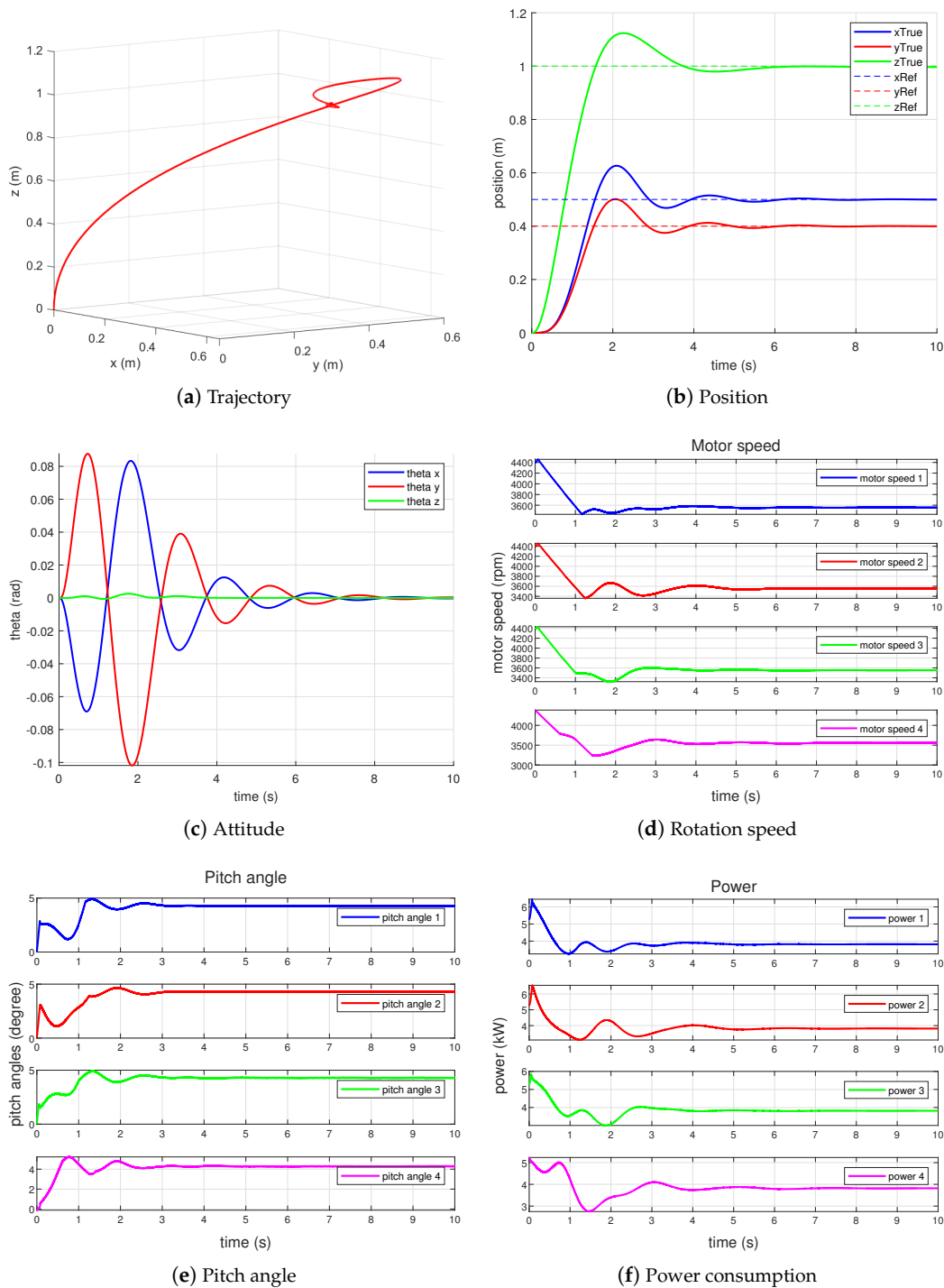


**Figure 9.** Set-point control using variable-pitch propellers.

Next, the same control algorithms are simulated under conditions  $\alpha = 5^\circ$  and  $\alpha = 10^\circ$  with the pitch angles of the four propellers remaining the same. The results for conditions  $\alpha = 5^\circ$  and  $\alpha = 10^\circ$  are shown in Figures 10 and 11, respectively. As for case  $\alpha = 5^\circ$ , which is higher than most angles shown in Figure 9, the controller fails to arrive at the given set-point despite the fact that the propellers are able to constantly offer sufficient force and torque for the aircraft platform. The main reason why the controller fails at this scenario

is that the four pitch angles are no longer controllable, which causes the robustness of the control allocation module to decrease dramatically. Then, the virtual pitch angle  $\alpha$  is continually increased to  $10^\circ$  against the proposal, meaning that the propeller system can finally arrive at the target stably. The position curve under this virtual situation is very close to that of the variable-pitch propellers in Figure 9, but the attitude curve develops differently. Nevertheless, since the force provided by this kind of propeller is larger than the proposed variable-pitch propellers, the ultimate mechanical power for each propeller is 4.5 kW, which is 20% higher.

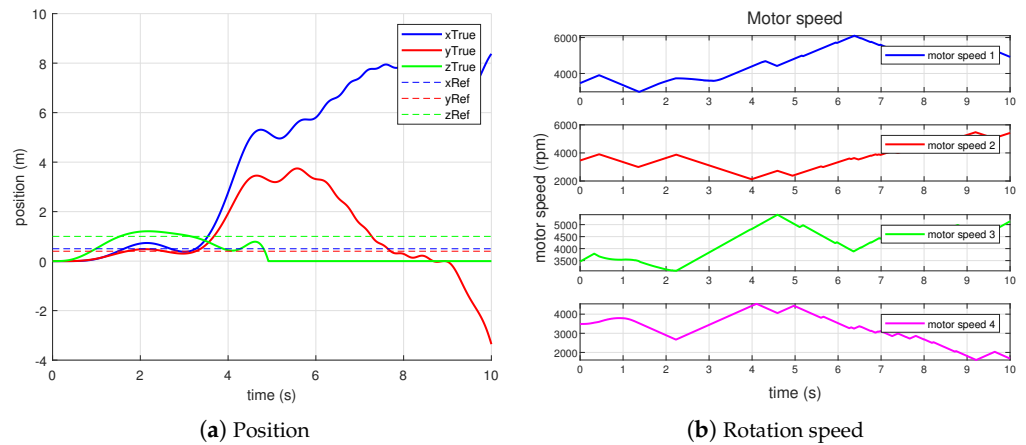


Figure 10. Set-point control using virtual pitch angle =  $5^\circ$  quadrotor.

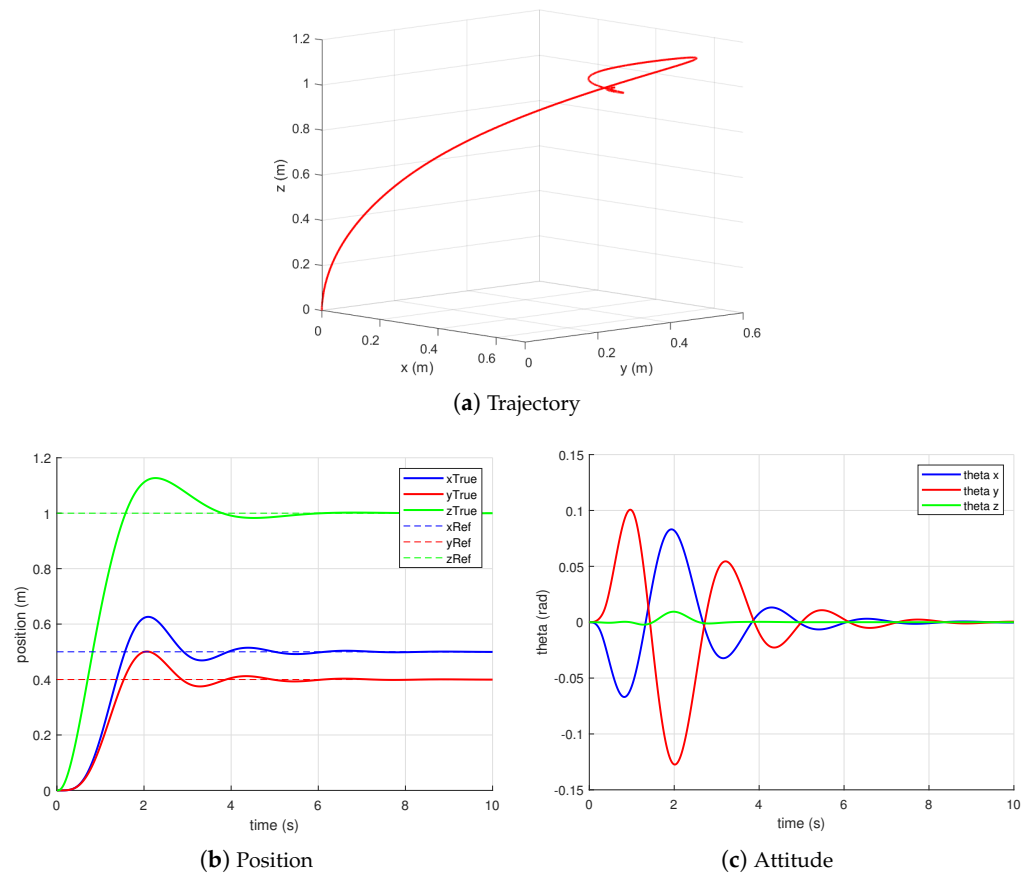


Figure 11. Cont.

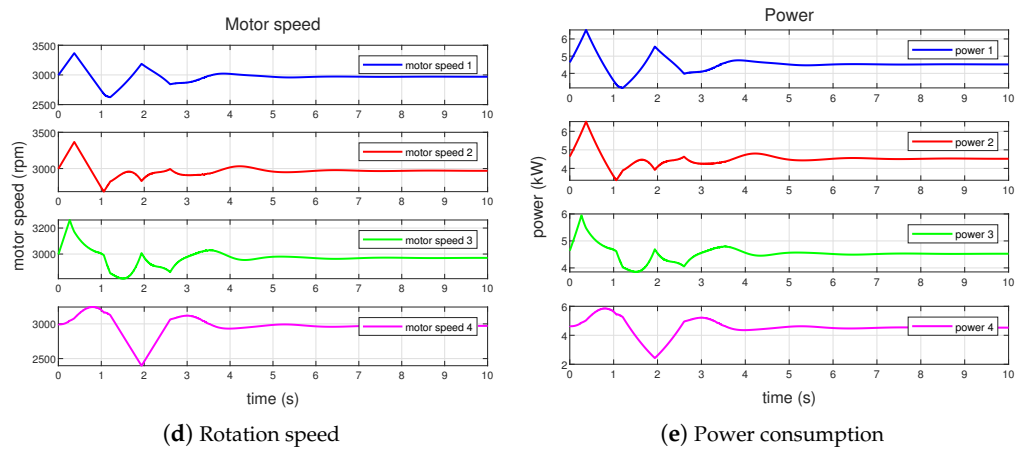


Figure 11. Set-point control using virtual pitch angle = 10° quadrotor.

#### 4.2. Aggressive Trajectory Tracking

A typical method to validate the effectiveness of a flight controller is to simulate whether it can track some aggressive trajectories. Different from quadrotors which are able to dance along some fascinating trajectories with extremely high speeds, large-scale eVTOLs pay more attention to the stability, robustness, and energy consumption of the system. As a result, a spiral ascent trajectory is defined as in Equation (31), which is indeed an exceedingly aggressive trajectory for large-scale eVTOLs.

$$\begin{cases} x = R \sin \frac{2\pi}{T}t \\ y = R \left( 1 - \cos \frac{2\pi}{T}t \right) \\ z = kt \end{cases} \quad (31)$$

where

$$R = 15m, T = 15s, k = 1m/s \quad (32)$$

The behavior of the designed control system is shown in Figure 12. Generally speaking, the proposed control system successfully tracks the given trajectory. From the results, it can be summarized that the controller utilizes all of the eight control variables to track the reference trajectory with an approximately 0.5 s time delay, which is common using a nonforward model-free controller structure such as cascade PID. The power curve is also constrained under 10 kW, which prevents the eVTOL from accidents due to there being insufficient power. Additionally, the dramatic changes in the four pitch angles demonstrate that the role of the variable-pitch controller is irreplaceable.

In contrast, the controller fails to track the given aggressive trajectory given motor parameters under the  $\alpha = 10^\circ$  condition, which explains that under a bunch of constraints such as energy consumption and the maximum change rate of rotation speed, it is not suitable to control such a large eVTOL aircraft by just using four motor speeds during the VTOL phase. The control results of this scenario are shown in Figure 13.

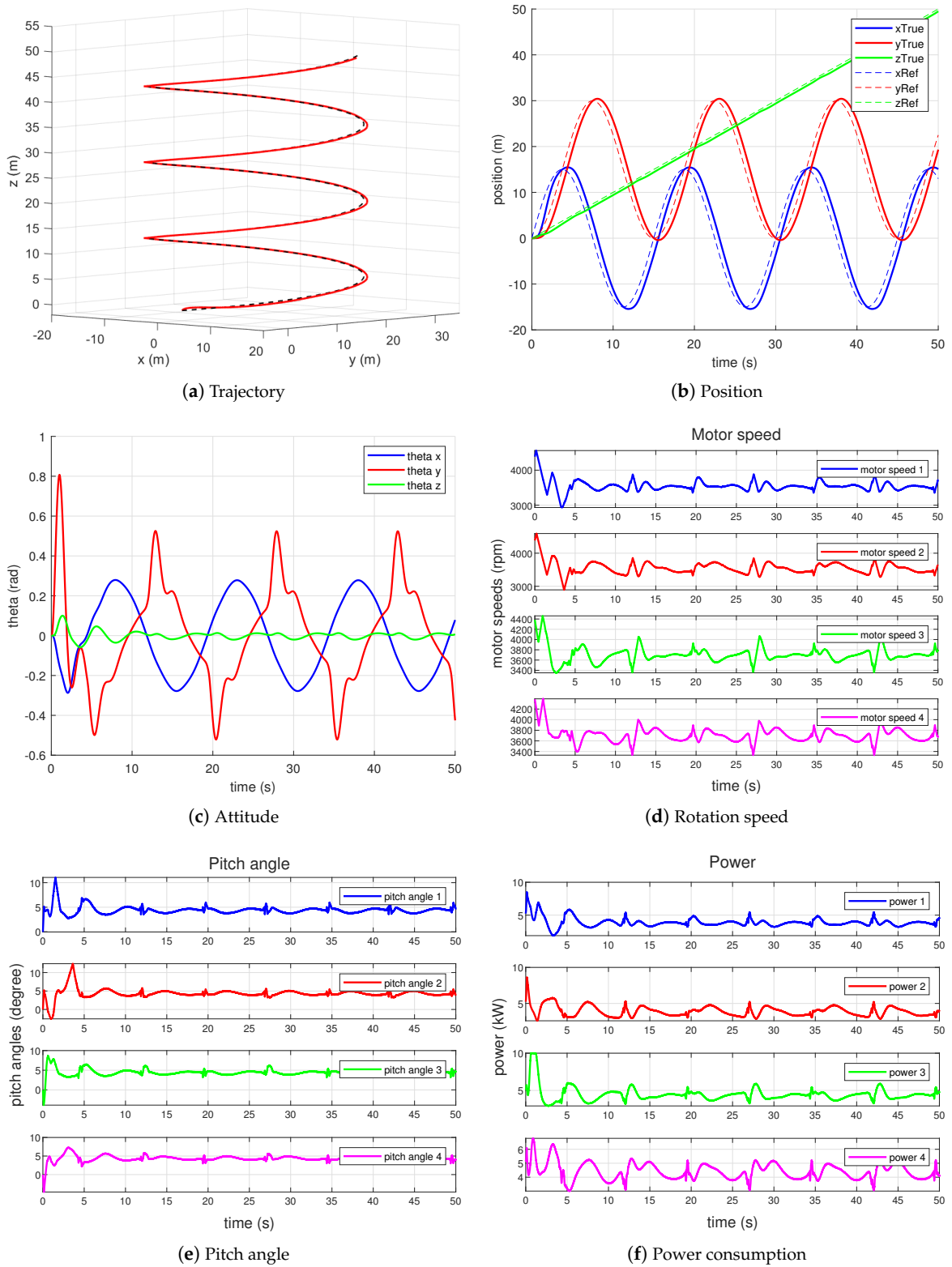


Figure 12. Aggressive trajectory tracking using variable-pitch propellers.

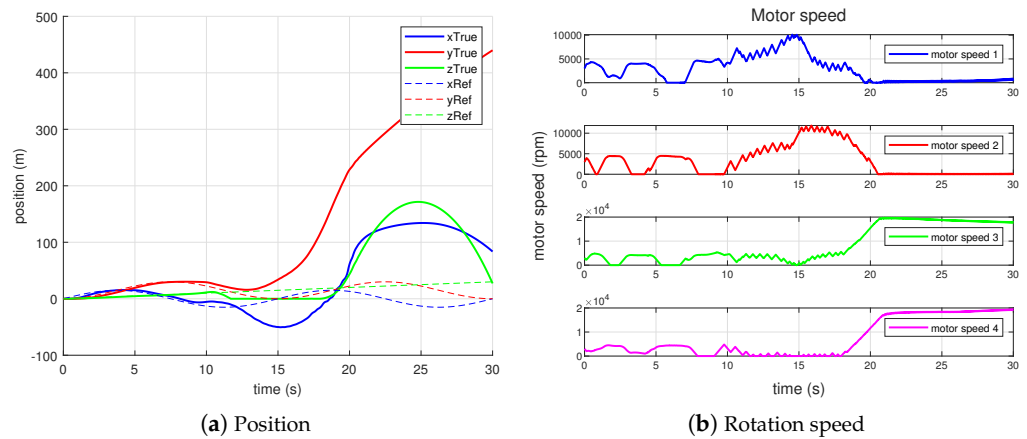


Figure 13. Aggressive trajectory tracking using virtual pitch angle = 10° quadrotor.

4.3. Flying Under Measurement Noise and External Disturbances

In this subsection, the efficiency of the proposed control algorithms is validated under significant measurement noise and external disturbances. The places where these noise and disturbances are introduced are depicted in Figure 14. The noisy measurement situation is introduced in advance since it is normally a common situation in real flight, followed by dramatic external disturbing forces. The amplitudes of white-noise error signals are listed in Table 2.

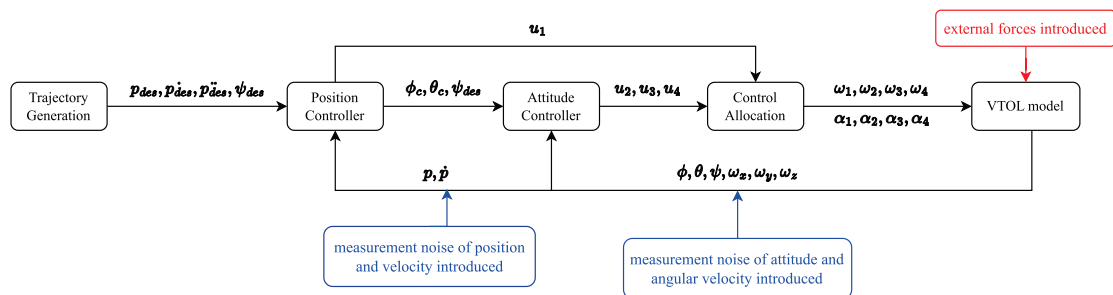


Figure 14. Control allocation module description.

Table 2. Measurement noise table described by the amplitudes of noise.

Parameter	Observation Error Amplitude
position ( $x, y, z$ )	$\pm 1.5$ [m]
attitude ( $\phi, \theta, \psi$ )	$\pm 20$ [deg]
velocity ( $v_x, v_y, v_z$ )	$\pm 0.4$ [m/s]
angular velocity ( $\omega_x, \omega_y, \omega_z$ )	$\pm 0.5$ [rad/s]

The results of adding the measurement noise situation are depicted in Figure 15, and the noises are provided from the Band-Limited White Noise block in MATLAB as shown in Figure 16. It can be concluded from the results that the controller is able to track the given aggressive trajectory with a similar time delay after adding relatively large measurement noise; thus, the robustness of the given controller can be proven. In addition, the mechanical power of each variable-pitch propeller is constrained under 10 kW, which guarantees the security of the flight even with some unexpected accidents occurring. Moreover, conclusions can be drawn from the pitch angle figure that the potential of pitch angle control has been fully motivated toward, which prevents the rotation speeds from changing so dramatically and causing harm that could have been avoided.

Finally, dramatic external forces are imposed on the aircraft as shown in Equation (33) with measurement noise added simultaneously. The behaviors are drawn in Figure 17 and

noise figures of the position and attitude are drawn in Figure 18. From the position curve, a dramatic change can be observed when external forces are imposed at 6–10 and 25–30 s, causing suddenly enormous shifting trends from the original position. Nevertheless, these positions quickly bounce back to the places where they should be, which illustrates the ability and robustness of the designed controller. Meanwhile, despite these disturbances, the mechanical powers of all four propellers are constrained to less than 10 kW, showing that it is possible to reduce energy consumption while tracking aggressive trajectories with acceptable accuracy at the same time with variable-pitch propellers as the actuator system.

$$F_x = \begin{cases} -200 & t \in [6, 10] \\ 300 & t \in [25, 30] \\ 0 & \text{other time} \end{cases} \quad F_y = \begin{cases} -300 & t \in [6, 10] \\ 400 & t \in [25, 30] \\ 0 & \text{other time} \end{cases} \quad F_z = \begin{cases} -400 & t \in [6, 10] \\ 500 & t \in [25, 30] \\ 0 & \text{other time} \end{cases} \quad (33)$$

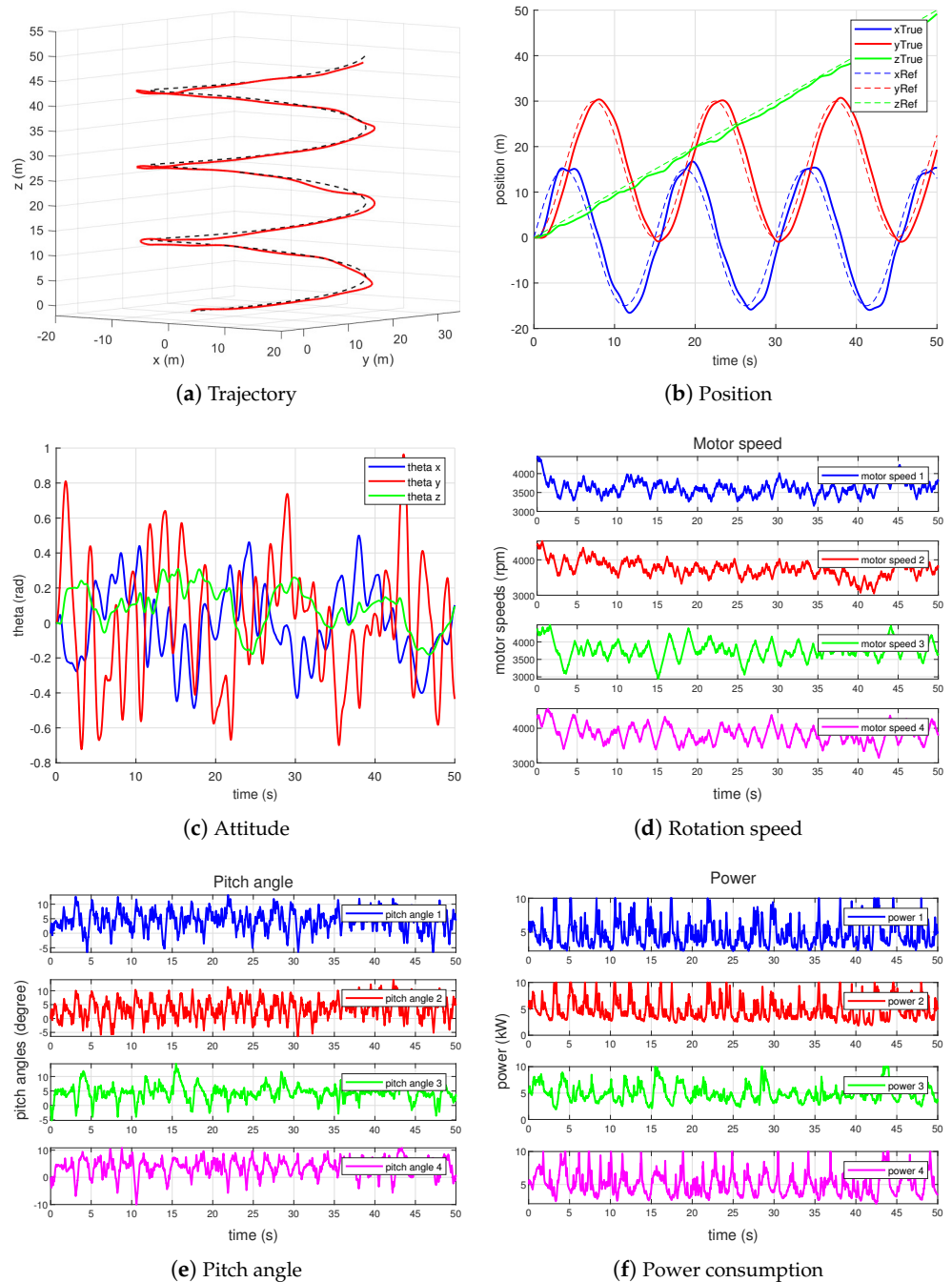


Figure 15. Aggressive trajectory tracking under measurement noise using variable-pitch propellers.



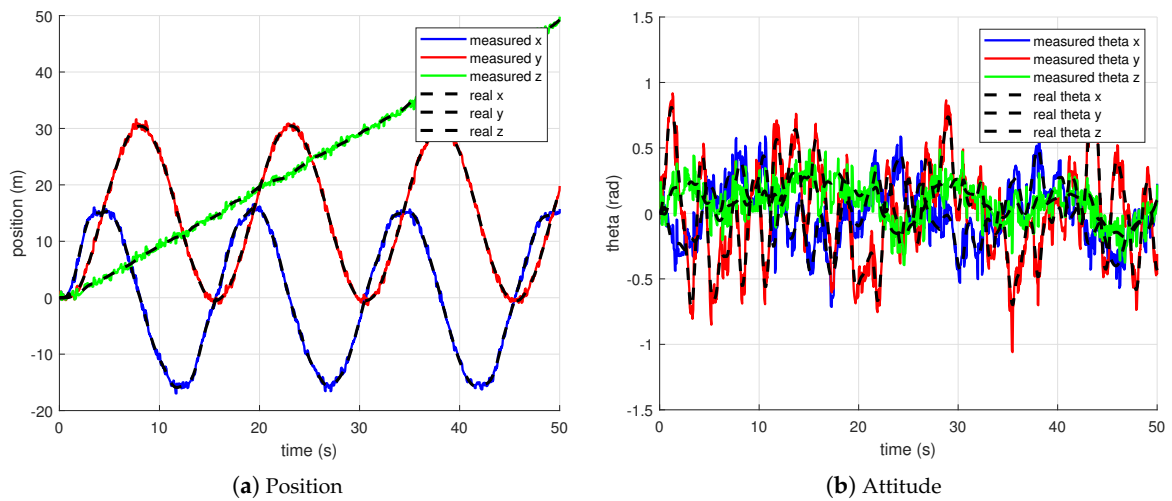


Figure 16. Real values and measured values of position and attitude with measurement noise.

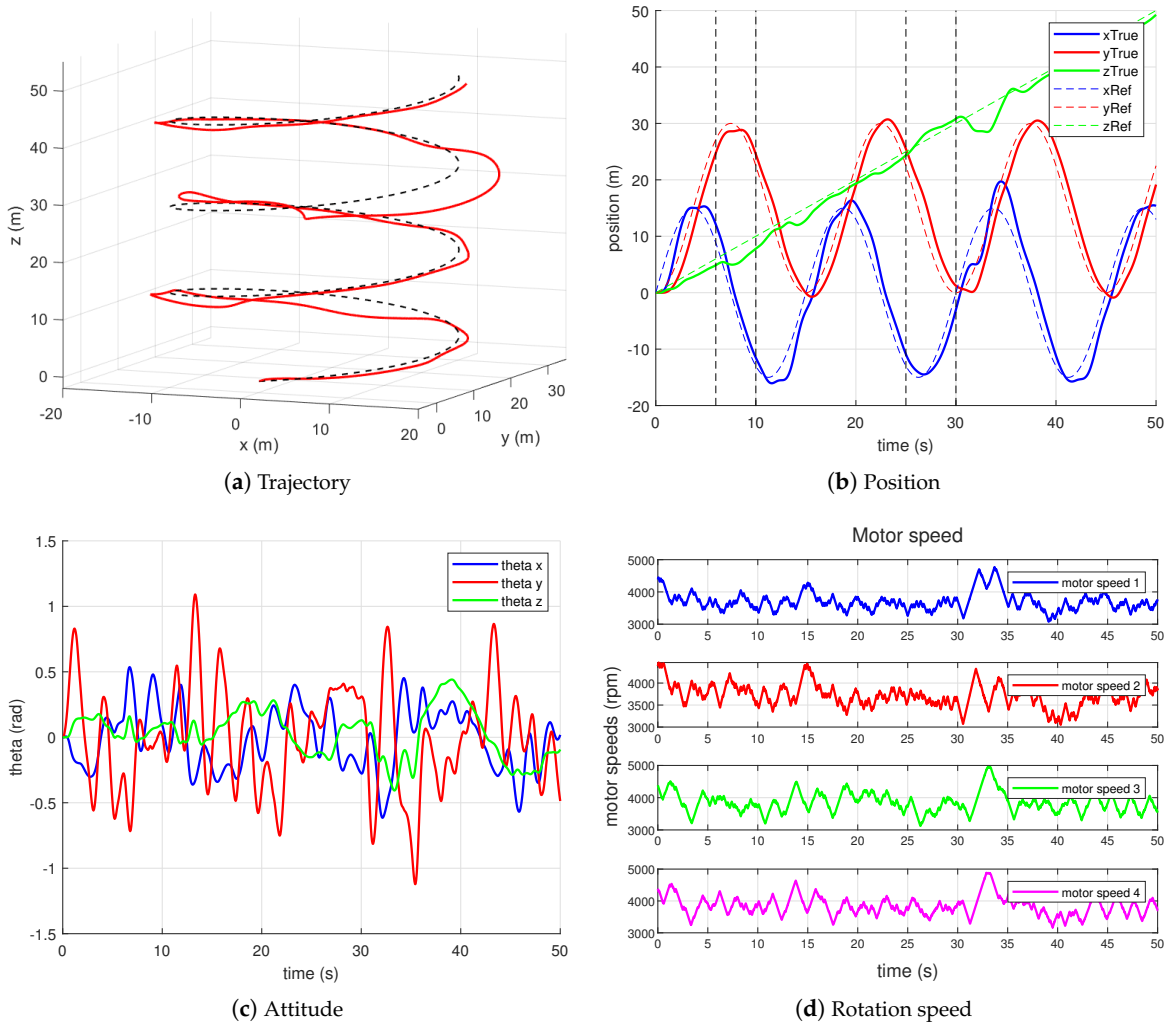
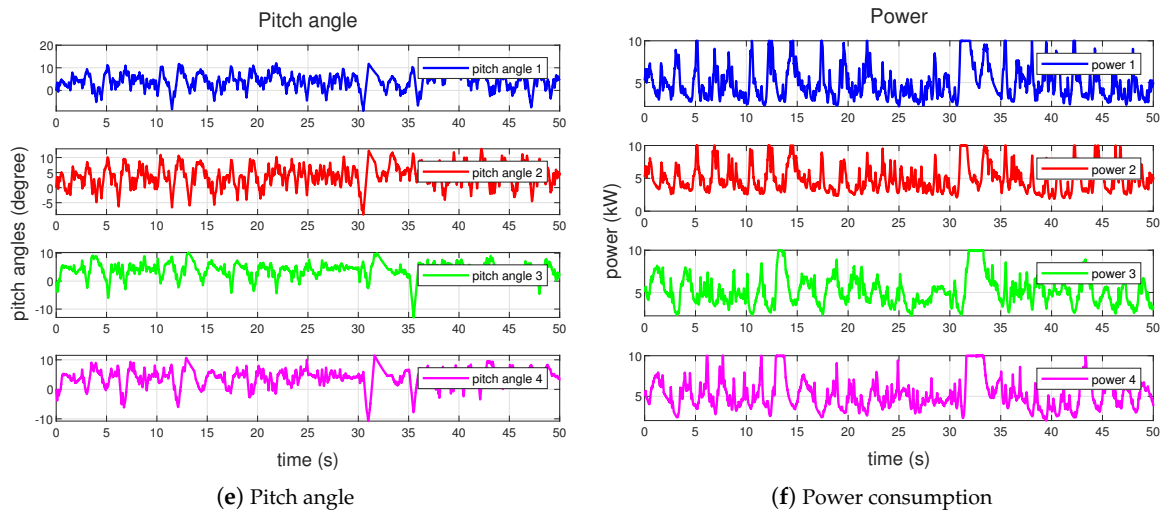
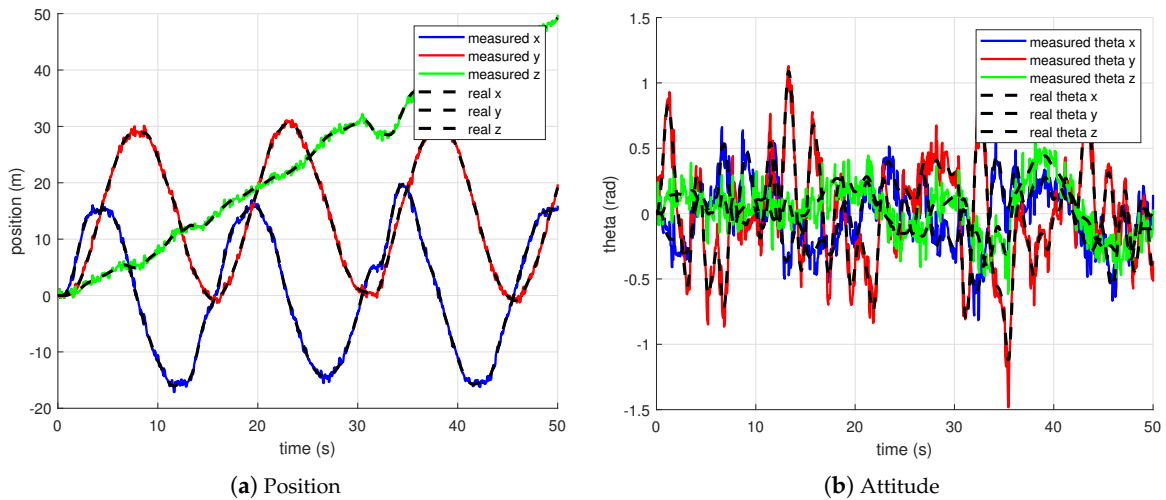


Figure 17. Cont.



**Figure 17.** Aggressive trajectory tracking under measurement noise and external forces using variable-pitch propellers.



**Figure 18.** Real values and measured values of position and attitude with measurement noise and external forces.

4.4. Numerical Analysis

4.4.1. Set-Point Control

Power indexes are established to compare the control performances between variable-pitch propellers and regular propellers with a virtual pitch of  $10^\circ$ . The numerical results are listed in Table 3.

**Table 3.** Power indexes of two situations when executing set-point control.

Index	Variable-Pitch Propellers	Regular Propellers with Virtual Pitch $10^\circ$
maximum power [kW]	6.3987	6.5036
stable power [kW]	3.7985	4.5021
average power [kW]	3.8609	4.5358

From Table 3, conclusions can be drawn that variable-pitch propellers require much less power than regular propellers when executing the set-point control mission using the eVTOL prototype. This is because the actual pitch angle of variable-pitch propellers is

maintained at around 5 degrees, which is much less than the virtual pitch of 10 degrees, while still being able to control the aircraft.

#### 4.4.2. Aggressive Trajectory Control

Under this scenario, a trajectory tracking error should be introduced to describe the validity of the designed control algorithms. The MSE is calculated to depict the tracking error during the flying process, which is shown in Equation (34).

$$\text{MSE} = \frac{1}{T_{\text{total}}} \int_0^{T_{\text{total}}} \|\mathbf{p} - \mathbf{p}_{\text{traj}}\|_2^2 dt \quad (34)$$

However, the MSE is only able to describe the absolute trajectory tracking error. Therefore, the target trajectory length is used to regularize the tracking error index. The length can be represented as

$$L = \sqrt{k^2 T_{\text{total}}^2 + (2\pi R)^2} \quad (35)$$

Consequently, the new numerical index AVGMSE describing the tracking error can be defined as

$$\text{AVGMSE} = \frac{\text{MSE}}{L^2} \quad (36)$$

The AVGMSE, maximum power, and average power are recognized as numerical indexes to describe the abilities of the control algorithm under the aggressive trajectory control scenario. Since the scenarios in Sections 4.2 and 4.3 are similar, the numerical results are listed together in Table 4.

**Table 4.** Numerical indexes of three situations when executing aggressive trajectory control.

Situation	AVGMSE	Maximum Power [kW]	Average Power [kW]
Aggressive trajectory tracking	$4.74 \times 10^{-3}$	10	4.0294
Aggressive trajectory tracking with noise	$5.67 \times 10^{-3}$	10	4.5643
Aggressive trajectory tracking with noise and disturbances	$6.75 \times 10^{-3}$	10	5.0322

From Table 4 conclusions can be drawn that the trajectory tracking error is acceptable even under measurement noise and external disturbances, proving the validity of the designed controller under the aggressive trajectory tracking scenario.

## 5. Conclusions

This paper presents the design and control framework of a set of variable-pitch propellers on a typical large-scale eVTOL during its VTOL phase. Both eVTOL and variable-pitch propeller platforms have been introduced in the first place, followed by controller arrangements and simulation experiments. It has been revealed in this paper that the controller is sufficiently stable and robust during the VTOL phase when tracking aggressive trajectories. The specific mechanism of variable-pitch propellers is also proven to have better control abilities than regular fixed pitch propellers when tracking these trajectories and overcoming unknown noise and disturbances. In conclusion, the concept of variable-pitch propellers used for large-scale eVTOLs to overcome the lack of propulsion has been universally acknowledged, and we believe that our findings could further enhance the abilities of variable-pitch propellers to realize high-performance flights, especially during the VTOL phase in the future.

However, it is worth mentioning that control algorithms concerning the cruise phase are not considered, which is crucial to the whole flying process. In our future work, more

exquisite controllers along with more comprehensive control allocation algorithms will be explored in order to fit both flying phases of the aircraft.

**Author Contributions:** Conceptualization, L.D. and Y.H.; methodology, L.D.; software, L.D.; validation, L.D. and Y.H.; formal analysis, L.D.; investigation, L.D. and Y.H.; resources, L.F.; data curation, L.D.; writing—original draft preparation, L.D.; writing—review and editing, L.D., Y.H., W.Q., G.W. and Y.X.; visualization, L.D. and Y.H.; supervision, L.F. and Y.H.; project administration, L.F., Y.H., W.Q., G.W. and Y.X.; funding acquisition, L.F. All authors have read and agreed to the published version of the manuscript.

**Funding:** This work is supported by the Intelligent Aerospace System Team of the Zhejiang Provincial Leading Innovative Teams Program, Science and Technology of Zhejiang Province (Grant No. 2022R01003).

**Data Availability Statement:** The data supporting reported results is complex and large. Researchers who are interested in our work can email me (heyunhan@foxmail.com) to get the data.

**Conflicts of Interest:** The authors declare no conflicts of interest.

## References

- Schumacher, L.; McNamee, P.I.; Haug, J.; Barrett, R. Development of a safe, quiet, certifiable personal vtol system. In Proceedings of the AIAA Aviation 2019 Forum, Dallas, TX, USA, 17–21 June 2019; p. 3475.
- Gu, H.; Lyu, X.; Li, Z.; Shen, S.; Zhang, F. Development and experimental verification of a hybrid vertical take-off and landing (VTOL) unmanned aerial vehicle (UAV). In Proceedings of the 2017 International Conference on Unmanned Aircraft Systems (ICUAS), Miami, FL, USA, 13–16 June 2017; pp. 160–169.
- Cetinsoy, E. Design and modeling of a gas-electric hybrid quad tilt-rotor UAV with morphing wing. In Proceedings of the 2014 IEEE International Conference on Mechatronics and Automation, Tianjin, China, 3–6 August 2014; pp. 1193–1198.
- Carlson, S. A hybrid tricopter/flying-wing vtol uav. In Proceedings of the 52nd Aerospace Sciences Meeting, National Harbor, MD, USA, 13–17 January 2014; p. 0016.
- Dickeson, J.J.; Miles, D.; Cifdaloz, O.; Wells, V.L.; Rodriguez, A.A. Robust lpv h gain-scheduled hover-to-cruise conversion for a tilt-wing rotorcraft in the presence of cg variations. In Proceedings of the 2007 American Control Conference, New York, NY, USA, 9–13 July 2007; pp. 5266–5271.
- Çetinsoy, E.; Sirimoğlu, E.; Öner, K.T.; Hancer, C.; Ünel, M.; Akşit, M.F.; Kandemir, I.; Gülez, K. Design and development of a tilt-wing UAV. *Turk. J. Electr. Eng. Comput. Sci.* **2011**, *19*, 733–741. [[CrossRef](#)]
- Lu, G.; Cai, Y.; Chen, N.; Kong, F.; Ren, Y.; Zhang, F. Trajectory Generation and Tracking Control for Aggressive Tail-Sitter Flights. *arXiv* **2022**, arXiv:2212.11552.
- Gu, H.; Cai, X.; Zhou, J.; Li, Z.; Shen, S.; Zhang, F. A coordinate descent method for multidisciplinary design optimization of electric-powered winged uavs. In Proceedings of the 2018 International Conference on Unmanned Aircraft Systems (ICUAS), Dallas, TX, USA, 12–15 June 2018; pp. 1189–1198.
- Cong, K.; Ma, D.; Zhang, L.; Xia, X.; Yao, Y. Design and analysis of passive variable-pitch propeller for VTOL UAVs. *Aerosp. Sci. Technol.* **2023**, *132*, 108063. [[CrossRef](#)]
- Cutler, M.; How, J.P. Analysis and control of a variable-pitch quadrotor for agile flight. *J. Dyn. Syst. Meas. Control* **2015**, *137*, 101002. [[CrossRef](#)]
- Cutler, M.; How, J. Actuator constrained trajectory generation and control for variable-pitch quadrotors. In Proceedings of the AIAA Guidance, Navigation, and Control Conference, Minneapolis, MN, USA, 13–16 August 2012; p. 4777.
- Xu, Z.; Fan, L.; Qiu, W.; Wen, G.; He, Y. A Robust Disturbance-Rejection Controller Using Model Predictive Control for Quadrotor UAV in Tracking Aggressive Trajectory. *Drones* **2023**, *7*, 557. [[CrossRef](#)]
- Portillo, P.; Garza-Castañón, L.E.; Minchala-Avila, L.I.; Vargas-Martínez, A.; Puig Cayuela, V.; Payeur, P. Robust Nonlinear Trajectory Controllers for a Single-Rotor UAV with Particle Swarm Optimization Tuning. *Machines* **2023**, *11*, 870. [[CrossRef](#)]
- Bianchi, D.; Borri, A.; Cappuzzo, F.; Di Gennaro, S. Quadrotor Trajectory Control Based on Energy-Optimal Reference Generator. *Drones* **2024**, *8*, 29. [[CrossRef](#)]
- Sheng, S.; Sun, C. Control and optimization of a variable-pitch quadrotor with minimum power consumption. *Energies* **2016**, *9*, 232. [[CrossRef](#)]
- Gebauer, J.; Wagnerová, R.; Smutný, P.; Podešva, P. Controller design for variable pitch propeller propulsion drive. *IFAC PapersOnLine* **2019**, *52*, 186–191. [[CrossRef](#)]
- Gupta, N.; Kothari, M. Flight dynamics and nonlinear control design for variable-pitch quadrotors. In Proceedings of the 2016 American Control Conference (ACC), Boston, MA, USA, 6–8 July 2016; pp. 3150–3155.
- Zhao, B.; Yue, D. Nonlinear robust control design for a miniature variable-pitch quadrotor. In Proceedings of the 2018 IEEE 14th International Conference on Control and Automation (ICCA), Anchorage, AK, USA, 12–15 June 2018; pp. 757–762.

19. Bristeau, P.J.; Martin, P.; Salaün, E.; Petit, N. The role of propeller aerodynamics in the model of a quadrotor UAV. In Proceedings of the 2009 European Control Conference (ECC), Budapest, Hungary, 23–26 August 2009; pp. 683–688.
20. Stevens, B.L.; Lewis, F.L.; Johnson, E.N. *Aircraft Control and Simulation: Dynamics, Controls Design, and Autonomous Systems*; John Wiley & Sons: Hoboken, NJ, USA, 2015.
21. Mellinger, D.; Kumar, V. Minimum snap trajectory generation and control for quadrotors. In Proceedings of the 2011 IEEE International Conference on Robotics and Automation, Shanghai, China, 9–13 May 2011; pp. 2520–2525.
22. Zhou, X.; Wang, Z.; Ye, H.; Xu, C.; Gao, F. Ego-planner: An esdf-free gradient-based local planner for quadrotors. *IEEE Robot. Autom. Lett.* **2020**, *6*, 478–485. [[CrossRef](#)]
23. Bertsekas, D.P. *Constrained Optimization and Lagrange Multiplier Methods*; Academic Press: Cambridge, MA, USA, 2014.
24. Wang, Z.; Gao, F. SDQP: Small-Dimensional Strictly Convex Quadratic Programming in Linear Time; 2022. Available online: <https://github.com/ZJU-FAST-Lab/SDQP> (accessed on 22 March 2024).

**Disclaimer/Publisher’s Note:** The statements, opinions and data contained in all publications are solely those of the individual author(s) and contributor(s) and not of MDPI and/or the editor(s). MDPI and/or the editor(s) disclaim responsibility for any injury to people or property resulting from any ideas, methods, instructions or products referred to in the content.